

# Frequency response and bandwidth analysis of multi-layer graphene nanoribbon and multi-walled carbon nanotube interconnects

Manoj Kumar Majumder, Narasimha Reddy Kukkam, Brajesh Kumar Kaushik

Department of Electronics and Communication Engineering, Indian Institute of Technology Roorkee, Roorkee 247667, India  
E-mail: manojbesu@gmail.com

Published in Micro & Nano Letters; Received on 2nd January 2014; Revised on 19th June 2014; Accepted on 20th June 2014

This reported research analyses and compares the bandwidth and absolute frequency response of a multi-layer graphene nanoribbon (MLGNR) and a multi-walled carbon nanotube (MWCNT) at local, semi-global and global interconnect lengths. The transfer function of the driver-interconnect-load system is obtained by representing the interconnect line with an equivalent single conductor model of either a MLGNR or a MWCNT. Using absolute frequency response, it is observed that the bandwidth of the MLGNR is higher by almost ten times and four times in comparison to the MWCNT for local and global interconnect lengths, respectively.

**1. Introduction:** During the recent past, multi-walled carbon nanotubes (MWCNTs) and multi-layer graphene nanoribbons (MLGNRs) have attracted much attention in scientific research because of their unique physical properties such as higher thermal conductivity, current carrying capability, mechanical strength and so on [1–3] in comparison to Cu interconnects. Both the MLGNR and MWCNT support large current densities up to  $10^9$  A/cm<sup>2</sup> and have long mean free paths ranging from 1 to 5  $\mu$ m. On the basis of chirality (rolled up direction of graphene sheets), MWCNTs and MLGNRs exhibit metallic as well as semiconducting properties. However, only the metallic nature is important for VLSI interconnect applications. The fabrication of a MLGNR is more controllable than for a MWCNT because of its planar nature [1, 2].

Previously, Cui *et al.* [3] derived an analytical expression of the output voltage waveform of a MLGNR interconnect. Nasiri *et al.* [4] also approximated the input–output transfer function of a MLGNR using the fourth-order Padé's approximation by assuming a driver resistance equal to zero ( $R_{dr}=0$ ) and perfect metal-MLGNR contacts ( $R_{mc}=0$ ). The authors plotted Nyquist diagrams for MLGNR lengths up to only the semi-global range. However, Fathi *et al.* [5] plotted the Nyquist diagrams of carbon nanotube (CNT) bundle interconnects by correctly assuming the driver parasitics and contact resistance only for local interconnects. In recent years, Nishad and Sharma [6] and Kumar and Naeemi [7] proposed analytical time and frequency domain models of side contact (SC) and top contact (TC) MLGNR interconnects. However, the authors neglected the driver resistance ( $R_{dr}$ ) and capacitance ( $C_{dr}$ ) while deriving the transfer function of SC and TC MLGNRs. While these previous works [3–7] demonstrate the potential advantages of either a MLGNR or a MWCNT interconnect separately, they do not provide a comprehensive comparison between the MLGNR and MWCNT interconnects for bandwidth and frequency response.

This Letter presents a comparative analysis of the frequency response and the bandwidth of MLGNR and MWCNT interconnects. To reduce the computational effort required for analysing the *RLC* circuit, a simplified but accurate equivalent single conductor (ESC) model is employed by considering an imperfect metal-MLGNR/MWCNT contact resistance ( $R_{mc}$ ). Using a driver-interconnect-load (DIL) system, a transfer function of the distributed transmission line is derived to obtain the bandwidth at local, semi-global and global interconnect lengths. The transfer function accurately takes into account the driver resistance ( $R_{dr}$ ) and capacitance ( $C_{dr}$ ).

**2. Interconnect model:** MLGNRs are considered as unrolled MWCNTs formed by hexagonal rings of carbon atoms. Owing to

the Vander-Waal's force between the neighbouring carbon atoms, the inter layer (or inter shell) distance of the MLGNR (or MWCNT) is  $\delta \approx 0.34$  nm [2]. Fig. 1 shows the cross-section of the side-contact MLGNR and MWCNT with an equivalent width and thickness (or diameter) of  $w$  and  $t$  (or  $d$ ), respectively. The total number of layers ( $N_{layer}$ ) and shells ( $N_{shell}$ ) in the MLGNR and MWCNT primarily depends on the  $w$ ,  $t$  and outer shell diameter ( $d$ ), respectively. Therefore, the areas of the MLGNR and MWCNT are obtained as  $w \cdot t$  and  $\pi(d/2)^2$ , respectively. Depending on the geometry, the ESC model of either the MLGNR or MWCNT is used to represent the interconnect line of the DIL in Fig. 2. The driver resistance, driver capacitance and the load capacitance are represented as  $R_{dr}$ ,  $C_{dr}$  and  $C_L$ , respectively.

The interconnect parasitics (i.e. resistance, inductance and capacitance) are modelled using the number of conducting channels ( $N_{ch}$ ) of each layer (or shell) in the MLGNR (or MWCNT).  $N_{ch}$  takes into account the effect of spin and sub-lattice degeneracy of carbon atoms and depends on the number of sub-bands, Fermi energy, temperature and the dimensions of the MLGNR and MWCNT interconnects [8, 9].  $N_{ch}$  of the MLGNR and MWCNT can be expressed as

$$N_{ch(MLGNR)} = c_0 + c_1 w + c_2 w^2 + c_3 E_F + c_4 w E_F + c_5 E_F^2 \quad (1)$$

and

$$N_{ch(MWCNT)} \simeq k_1 T D_i + k_2, \quad D_i > d_T/T \\ \simeq 2/3, \quad D_i \leq d_T/T \quad (2)$$

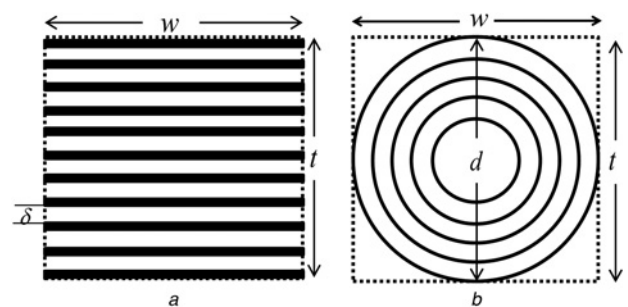


**Figure 1** Cross-section of MLGNR and MWCNT interconnect  
a MLGNR  
b MWCNT

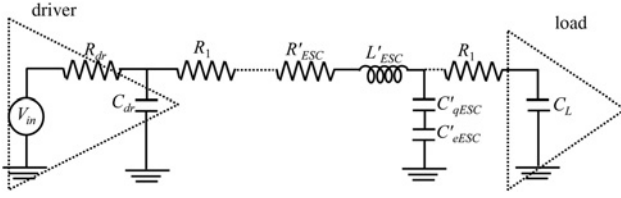


**Figure 2** DIL system representing the ESC model of MLGNR/MWCNT interconnects terminated by load capacitance  $C_L = 250$  aF

where  $c_0$  to  $c_5$  are the constant parameters for metallic GNRs at room temperature with the Fermi energy  $E_F > 0$  [8]. On the other hand,  $D_i$  represents the diameter of the  $i$ th shell in the MWCNT,  $k_1$  and  $k_2$  are equal to  $3.87 \times 10^{-4} \text{ nm}^{-1} \text{ K}^{-1}$  and 0.2, respectively [9]. The thermal energy of electrons and the gap between the sub-bands determine the quantitative value of  $d_T$  equivalent to 1300 nm.K at room temperature ( $T = 300$  K). Thus, the total number of conducting channels ( $N_{\text{total}}$ ) in a MLGNR (or MWCNT) is obtained by the summation of  $N_{\text{ch}}$  of each layer (or shell).

The lumped resistance ( $R_1$ ) in Fig. 2 is the series combination of imperfect metal-MLGNR/MWCNT contact resistance ( $R_{\text{mc}}$ ) and quantum resistance ( $R_q$ ). Depending on the fabrication process,  $R_{\text{mc}}$  exhibits a typical value of 3.2 k $\Omega$ . Resistance,  $R_q$  appears mainly because of the quantum confinement of electrons and depends on the number of conducting channels of each layer (or shell) in the MLGNR (or MWCNT) interconnects. In addition, the scattering resistance ( $R'_{\text{ESC}}$ ) is because of the static impurity scattering, defects, line edge roughness scattering and primarily depends on the effective mean free path ( $\lambda_{\text{mfp}}$ ) of electrons [3]. The lumped  $R_1$  and per unit length ( $p.u.l.$ )  $R'_{\text{ESC}}$  can be expressed as

$$R_1 = \left( R_{\text{mc}} + \frac{R_q}{N_{\text{total}}} \right) / 2; \quad \text{where} \quad R_q = \frac{h}{2e^2} \quad (3)$$

$$R'_{\text{ESC}} = \frac{h/2e^2}{2N_{\text{total}}\lambda_{\text{mfp}}}; \quad \text{where} \quad (4)$$

$$\lambda_{\text{mfp},i} = \frac{10^3 D_i}{(T/T_0) - 2}, \quad T_0 = 100 \text{ K}$$

The total inductance ( $L'_{\text{ESC}}$ ) of the MLGNR and MWCNT in Fig. 1 is the summation of kinetic ( $L'_{\text{kESC}}$ ) and magnetic ( $L'_{\text{eESC}}$ ) inductances that primarily represent the stored energy in the magnetic field and the inertial mass of mobile charge carriers, respectively [3, 9]. The effective  $p.u.l.$   $L'_{\text{ESC}}$  can be expressed as

$$L'_{\text{ESC}} = L'_{\text{kESC}} + L'_{\text{eESC}} \quad (5)$$

where

$$L'_{\text{kESC}} = \frac{L'_{\text{k0}}}{2N_{\text{total}}}; \quad L'_{\text{k0}} = \frac{h}{2e^2 v_F} \quad (6)$$

and

$$L'_{\text{eESC}} = \frac{\mu_0 \epsilon_0}{C'_{\text{eESC}}} \quad (7)$$

where  $v_F$  represents the Fermi velocity of the CNT and graphene  $\approx 8 \times 10^5$  and  $C'_{\text{eESC0}}$  is the effective electrostatic capacitance of the ESC embedded in free space.

The outermost layer (or shell) of the MLGNR (or MWCNT) experiences an electrostatic capacitance ( $C'_{\text{eESC}}$ ) with respect to the ground that appears in series with the quantum capacitance ( $C'_{\text{qESC}}$ ) shown in Fig. 2. Thus, the effective  $p.u.l.$  equivalent

**Table 1** Equivalent parasitics of MLGNR and MWCNT interconnects

Interconnect parasitic	Parasitic values at $t = d = 13.92$ nm	
	MLGNR	MWCNT
$R'_{\text{ESC}}, \Omega/\mu\text{m}$	150	21
$L'_{\text{ESC}}, \text{nH}/\mu\text{m}$	0.097	0.056
$C'_{\text{ESC}}, \text{aF}/\mu\text{m}$	6.74	89.78
$R_1, \text{k}\Omega$	1.614	1.612
$R_{\text{dr}}, \Omega$	292.36	
$C_{\text{dr}}, \text{aF}$	45.51	

capacitance ( $C'_{\text{ESC}}$ ) can be expressed as

$$C'_{\text{ESC}} = \left( 1/C'_{\text{qESC}} + 1/C'_{\text{eESC}} \right)^{-1} \quad (8)$$

$$C'_{\text{eESC,MLGNR}} = \frac{\epsilon_0 \epsilon_r w}{H}; \quad C'_{\text{eESC,MWCNT}} = \frac{2\pi \epsilon_0 \epsilon_r}{\cosh^{-1}(H/d)} \quad (9)$$

$$C'_{\text{qESC}} = 2N_{\text{total}}C'_{\text{q0}}; \quad \text{where} \quad C'_{\text{q0}} = \frac{2e^2}{h v_F} \quad (10)$$

where  $\epsilon_r \approx 2.2$  and  $H$  represent the dielectric permittivity and the distance between the outermost layer (or shell) of the MLGNR (or MWCNT) and the ground plane, respectively. For a fixed  $t = d = 13.92$  nm, the quantitative values of the driver and interconnect parasitics of the MLGNR and the MWCNT are summarised in Table 1. The interconnect parasitics are primarily dependent on  $N_{\text{total}}$  and obtained using the parasitics expressions (1)–(10).

**3. Distributed transfer function of DIL system:** Transfer function of the DIL (Fig. 2) is obtained using the driver parasitics and the MLGNR and MWCNT interconnect parasitics (Table 1). To obtain the overall gain ( $V_{\text{out}}/V_{\text{in}}$ ), the DIL of Fig. 2 is represented as a cascaded connection of several two-port networks (Fig. 3). The best choice of the two-port parameter is the ABCD parameter. The ABCD matrix parameters of each two-port network are represented as  $g_1, g_2, g_3, g_4$  and  $g_5$ . The Telegrapher's equation of distributed transmission line [5, 10] is used to obtain the ABCD matrix parameter (gain)  $g_4$ . Using this method, the voltage and current at any point  $x$  of the DIL can be expressed as

$$\frac{\partial V}{\partial x} = -(R'_{\text{ESC}} + sL'_{\text{ESC}})I(x) \quad \text{and} \quad \frac{\partial I}{\partial x} = -sC'_{\text{ESC}} \cdot V(x) \quad (11)$$

Solving expression (11)

$$V = V_0 \cosh(\gamma nx) + I_0 Z_0 \sinh(\gamma nx) \quad (12a)$$

and

$$I = I_0 \cosh(\gamma nx) + V_0/Z_0 \sinh(\gamma nx) \quad (12b)$$

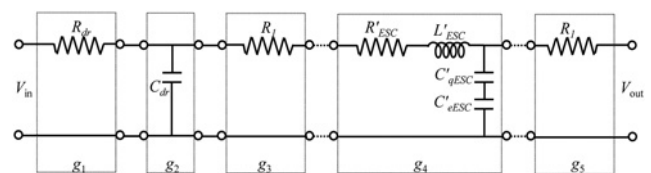


**Figure 3** Cascaded connection of the DIL of Fig. 2

Thus

$$\begin{bmatrix} V \\ I \end{bmatrix} = \begin{bmatrix} \cosh(\gamma nx) & Z_0 \sinh(\gamma nx) \\ 1/Z_0 \sinh(\gamma nx) & \cosh(\gamma nx) \end{bmatrix} \begin{bmatrix} V_0 \\ I_0 \end{bmatrix} \quad (13)$$

where  $n$ ,  $x$  and  $\gamma = \sqrt{sC'_{\text{ESC}}(R'_{\text{ESC}} + sL'_{\text{ESC}})}$  are the number of distributed segments, length of each segment and the propagation constant, respectively.

Using the transmission matrix parameter for a uniform  $RLC$  transmission line of length  $l$  [5, 10], the resultant transmission matrix parameter of the DIL configuration (Fig. 3) can be expressed as

$$\begin{aligned} T_{\text{result}} &= g_1 \cdot g_2 \cdot g_3 \cdot g_4 \cdot g_5 \\ &= \begin{bmatrix} 1 & R_{\text{dr}} \\ 0 & 1 \end{bmatrix} \begin{bmatrix} 1 & 0 \\ sC_{\text{dr}} & 1 \end{bmatrix} \begin{bmatrix} 1 & R_1 \\ 0 & 1 \end{bmatrix} \\ &\times \begin{bmatrix} \cosh(\gamma nx) & Z_0 \sinh(\gamma nx) \\ 1/Z_0 \sinh(\gamma nx) & \cosh(\gamma nx) \end{bmatrix} \begin{bmatrix} 1 & R_1 \\ 0 & 1 \end{bmatrix} = \begin{bmatrix} A & B \\ C & D \end{bmatrix} \end{aligned} \quad (14)$$

Now, using expression (14), the distributed transfer function of the DIL (Fig. 2) can be expressed as

$$\frac{V_{\text{out}}}{V_{\text{in}}} = \text{TF} = \frac{1}{A + sC_L B} \quad (15)$$

where

$$\begin{aligned} A &= 1 + s \left[ \frac{R'_{\text{ESC}} C'_{\text{ESC}}(nx)^2}{2} + R_{\text{dr}} C_{\text{dr}} + C'_{\text{ESC}}(nx)(R_1 + R_{\text{dr}}) \right] \\ &+ s^2 \left[ \frac{L'_{\text{ESC}} C'_{\text{ESC}}(nx)^2}{2} + \frac{R'^2_{\text{ESC}} C'^2_{\text{ESC}}(nx)^4}{4!} + \frac{R'_{\text{ESC}} R_{\text{dr}} C'_{\text{ESC}} C_{\text{dr}}(nx)^2}{2} \right. \\ &\left. + \frac{R'_{\text{ESC}} C'^2_{\text{ESC}}(nx)^3 (R_1 + R_{\text{dr}})}{3!} + R_1 R_{\text{dr}} C_{\text{dr}} C'_{\text{ESC}}(nx) \right] \end{aligned} \quad (15a)$$

(see (15b))

**4. Cutoff frequency and bandwidth analysis:** The transfer function of (15) is used to analyse the cutoff frequency ( $f_c$ ) that primarily depends on the MLGNR and MWCNT interconnect parasitics presented in Table 1. The parasitic values are obtained for similar diameters of the MWCNT and thicknesses of the MLGNR interconnects. To obtain the analytical and thicknesses of the cutoff frequency of the DIL, the transfer function of (15) can be

**Table 2** Bandwidth of MLGNR and MWCNT interconnects

$l$ , $\mu\text{m}$	$t=d$ , nm	MLGNR bandwidth, GHz		MWCNT bandwidth, GHz	
		Absolute	Analytical, second order	Absolute	Analytical, second order
5	7.12	36.4	36.26	19	18.88
	10.52	44.4	44.59	20.6	20.53
	13.92	63.3	63.36	45.1	44.67
500	7.12	2.25	2.20	0.04	0.04
	10.52	3.09	3.08	0.68	0.68
	13.92	3.5	3.48	1.5	1.49
2500	7.12	0.11	0.11	0.001	0.001
	10.52	0.14	0.14	0.02	0.02
	13.92	3.5	3.48	0.06	0.06

expressed to a simplified second-order expression as

$$\text{TF} = \frac{1}{a_0 + a_1 s + a_2 s^2} \quad (16a)$$

where  $a_0 = 1$ .

$$\begin{aligned} a_1 &= \left( \frac{R'_{\text{ESC}} C'_{\text{ESC}}(nx)^2}{2} + R_{\text{dr}} C_{\text{dr}} + C'_{\text{ESC}}(nx)(R_1 + R_{\text{dr}}) \right) \\ &+ C_L (2R_1 + R_{\text{dr}} + R'_{\text{ESC}}(nx)) \end{aligned} \quad (16b)$$

$$\begin{aligned} a_2 &= \left[ \frac{L'_{\text{ESC}} C'_{\text{ESC}}(nx)^2}{2} + \frac{R'^2_{\text{ESC}} C'^2_{\text{ESC}}(nx)^4}{4!} + \frac{R'_{\text{ESC}} R_{\text{dr}} C'_{\text{ESC}} C_{\text{dr}}(nx)^2}{2} \right. \\ &+ \frac{R'_{\text{ESC}} C'^2_{\text{ESC}}(nx)^3 (R_1 + R_{\text{dr}})}{3!} + R_1 R_{\text{dr}} C_{\text{dr}} C'_{\text{ESC}}(nx) \left. \right] \\ &+ C_L \left[ \frac{R'_{\text{ESC}} C'_{\text{ESC}}(nx)^2}{2} (2R_1 + R_{\text{dr}}) + 2R_1 R_{\text{dr}} C_{\text{dr}} + \frac{R'^2_{\text{ESC}} C'^2_{\text{ESC}}(nx)^3}{3!} \right. \\ &\left. + L'_{\text{ESC}}(nx) + R'^2_1 C'_{\text{ESC}}(nx) + R'_{\text{ESC}} R_{\text{dr}} C_{\text{dr}}(nx) + R_1 R_{\text{dr}} C'_{\text{ESC}}(nx) \right] \end{aligned} \quad (16c)$$

The roots of (16) can be expressed as

$$s_1 = \frac{-a_1 + \sqrt{a_1^2 - 4a_2}}{2a_2}$$

and

$$s_2 = \frac{-a_1 - \sqrt{a_1^2 - 4a_2}}{2a_2}$$

$$\begin{aligned} B &= (2R_1 + R_{\text{dr}} + R'_{\text{ESC}}(nx)) + s \left[ \frac{R'_{\text{ESC}} C'_{\text{ESC}}(nx)^2}{2} (2R_1 + R_{\text{dr}}) + 2R_1 R_{\text{dr}} C_{\text{dr}} \right. \\ &+ \frac{R'^2_{\text{ESC}} C'^2_{\text{ESC}}(nx)^3}{3!} + L'_{\text{ESC}}(nx) + R'^2_1 C'_{\text{ESC}}(nx) + R'_{\text{ESC}} R_{\text{dr}} C_{\text{dr}}(nx) + R_1 R_{\text{dr}} C'_{\text{ESC}}(nx) \left. \right] \\ &+ s^2 \left[ (2R_1 + R_{\text{dr}}) \left( \frac{L'_{\text{ESC}} C'_{\text{ESC}}(nx)^2}{2} + \frac{R'^2_{\text{ESC}} C'^2_{\text{ESC}}(nx)^4}{4!} \right) + R_1 R_{\text{dr}} R'_{\text{ESC}} C'_{\text{ESC}} C_{\text{dr}}(nx)^2 \right. \\ &+ \frac{2R'_{\text{ESC}} L'_{\text{ESC}} C'_{\text{ESC}}(nx)^3}{3!} + \frac{R'^3_{\text{ESC}} C'^3_{\text{ESC}}(nx)^5}{5!} + \frac{R'^2_1 R'_{\text{ESC}} C'^2_{\text{ESC}}(nx)^3}{3!} \\ &\left. + \frac{R'^2_{\text{ESC}} R_{\text{dr}} C_{\text{dr}} C'_{\text{ESC}}(nx)^3}{3!} + R_{\text{dr}} C_{\text{dr}} (L'_{\text{ESC}} + R'^2_1 C'_{\text{ESC}})(nx) \right] \end{aligned} \quad (15b)$$

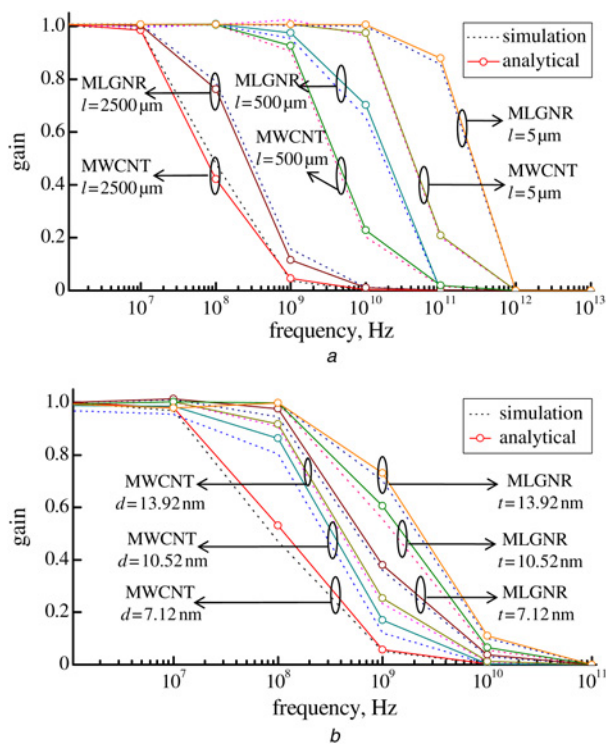


**Figure 4** Frequency response of MLGNR and MWCNT  
a For different interconnect lengths at  $t = d = 13.92$  nm  
b For different thickness and diameter at  $l = 2500$   $\mu\text{m}$

The cutoff frequency can be expressed as

$$f_c = \frac{1}{2\pi} \sqrt{\frac{(2a_2 - a_1^2) + \sqrt{(2a_2 - a_1^2)^2 + 4a_2^2}}{2a_2^2}} \quad (17)$$

Table 2 compares the bandwidth of the MLGNR and MWCNT obtained from the absolute frequency response of higher order and the analytical expression of reduced order (17). It is observed that bandwidths using both the methodologies are in good agreement with each other for the MLGNR and MWCNT interconnects. Apart from this, the bandwidth of both the MLGNR and MWCNT substantially reduces for longer interconnects. The reduction in bandwidth follows an exponentially decaying function and can be expressed through curve fitting as

$$\text{Bandwidth} = 1 + 2 \times \exp(-\text{length}) \quad (18)$$

Using the analytical expression of (17), the frequency response of the DIL is compared with the HSPICE-RF simulated results for

different interconnect lengths ( $l$ ), MLGNR thickness ( $t$ ) and MWCNT diameter ( $d$ ) as shown in Figs. 4a and b. The obtained results are in good agreement with each other. However, irrespective of interconnect lengths, it is observed that the MWCNT exhibits a lower  $f_c$  in comparison to the MLGNR. This fact can be explained in terms of dominating interconnect parasitics  $R'_{\text{ESC}}$  and  $C'_{\text{ESC}}$ . It leads to form an RC lowpass filter that has a bandwidth close to the cutoff frequency,  $f_c = 1/2\pi R'_{\text{ESC}} C'_{\text{ESC}}$ . For similar interconnect dimension, the time constant ( $R'_{\text{ESC}} C'_{\text{ESC}}$ ) of the MWCNT is higher compared with the MLGNR (Table 1) which results in a lower  $f_c$  for MWCNT interconnects. Therefore, irrespective of interconnect dimensions, the bandwidth of the MWCNT is alarmingly smaller by almost ten times and four times for local and global interconnects, respectively, in comparison to the MLGNR.

**5. Conclusion:** This Letter presents a comparative analysis of the frequency response and bandwidth of MLGNR and MWCNT interconnects. Using the DIL system, represented by the ESC model of MLGNR/MWCNT interconnects the transfer function is derived that is further used to obtain the cutoff frequency and bandwidth. It is observed that the MLGNR exhibits higher bandwidth compared with the MWCNT for various interconnect dimensions.

## 6 References

- [1] Li H., Xu C., Srivastava N., Banerjee K.: 'Carbon nanomaterials for next-generation interconnects and passives: physics, status, and prospects', *IEEE Trans. Electron Devices*, 2009, **56**, (9), pp. 1799–1820
- [2] Xu C., Li H., Banerjee K.: 'Modeling, analysis, and design of graphene nanoribbon interconnects', *IEEE Trans. Electron Devices*, 2009, **56**, (8), pp. 1567–1578
- [3] Cui J.-P., Zhao W.-S., Yin W.-Y.: 'Signal transmission analysis of multilayer graphene nano-ribbon (MLGNR) interconnects', *IEEE Trans. Electromag. Compat.*, 2012, **54**, (1), pp. 126–132
- [4] Nasiri S.H., Moravvej-Farshi Md.K., Faez R.: 'Stability analysis in graphene nanoribbon interconnects', *IEEE Electron Device Lett.*, 2010, **31**, (12), pp. 1458–1460
- [5] Fathi D., Forouzandeh B., Mohajerzadeh S., Sarvari R.: 'Accurate analysis of carbon nanotube interconnects using transmission line model', *Micro Nano Lett.*, 2009, **4**, (2), pp. 116–121
- [6] Nishad A.K., Sharma R.: 'Analytical time-domain models for performance optimization of multilayer GNR interconnects', *IEEE J. Sel. Top. Quantum Electron.*, 2014, **20**, (1), p. 3700108
- [7] Kumar V., Naeemi A.: 'Analytical models for the frequency response of multi-layer graphene nanoribbon interconnects'. Proc. IEEE Int. Symp. Electromagnetic Compatibility (EMC'12), 2012, pp. 440–445
- [8] Nasiri S.H., Faez R.: 'Compact formulae for number of conduction channels in various types of graphene nanoribbons at various temperatures', *Mod. Phys. Lett. B*, 2012, **26**, (1), pp. 11500041–1150045
- [9] Naeemi A., Meindl J.D.: 'Performance modeling for single- and multiwall carbon nanotubes as signal and power interconnects in gigascale systems', *IEEE Trans. Electron Devices*, 2008, **55**, (10), pp. 2574–2582
- [10] Sadiku M.N.O.: 'Elements of electromagnetics' (Oxford university Press, USA, 2009, 5th edn)